Applied Physics Letters

Engineering the gain-bandwidth product of phototransistor diodes

Cite as: Appl. Phys. Lett. **115**, 051104 (2019); https://doi.org/10.1063/1.5095815
Submitted: 13 March 2019 . Accepted: 11 July 2019 . Published Online: 30 July 2019

Simone Bianconi, Mohsen Rezaei, Min-Su Park, Wenyuan Huang, Chee Leong Tan, and Hooman Mohseni

Applied Physics Letters ARTICLE scitation.org/journal/apl

Engineering the gain-bandwidth product of phototransistor diodes

Cite as: Appl. Phys. Lett. **115**, 051104 (2019); doi: 10.1063/1.5095815
Submitted: 13 March 2019 · Accepted: 11 July 2019 ·
Published Online: 30 July 2019

Simone Bianconi,[1,a] Mohsen Rezaei,[1,a] Min-Su Park,[1,2] Wenyuan Huang,[1] Chee Leong Tan,[1,3] and Hooman Mohseni[1,b]

AFFILIATIONS

[1]Bio-Inspired Sensors and Optoelectronics Laboratory, Northwestern University, 2145 Sheridan Rd, Evanston, Illinois 60208, USA
[2]Nano Convergence Research Center, Korea Electronics Technology Institute (KETI), 111, Ballyong-ro, Deokjin-gu, Jeonju-si, Jeollabuk-do 54853, South Korea
[3]Photonics Research Center, University of Malaya, 50603 Kuala Lumpur, Malaysia

[a]**Contributions:** S. Bianconi and M. Rezaei contributed equally to this work.
[b]**Author to whom correspondence should be addressed:** hmohseni@northwestern.edu. **URL:** http://www.bisol.northwestern.edu

ABSTRACT

In recent years, phototransistors have considerably expanded their field of application, including for instance heterodyne detection and optical interconnects. Unlike in low-light imaging, some of these applications require fast photodetectors that can operate in relatively high light levels. Since the gain and bandwidth of phototransistors are not constant across different optical powers, the devices that have been optimized for operation in low light level cannot effectively be employed in different technological applications. We present an extensive study of the gain and bandwidth of short-wavelength infrared phototransistors as a function of optical power level for three device architectures that we designed and fabricated. The gain of the photodetectors is found to increase with increasing carrier injection. Based on a Shockley-Read-Hall recombination model, we show that this is due to the saturation of recombination centers in the phototransistor base layer. Eventually, at a higher light level, the gain drops, due to the Kirk effect. As a result of these opposing mechanisms, the gain-bandwidth product is peaked at a given power level, which depends on the device design and material parameters, such as doping and defect density. Guided by this physical understanding, we design and demonstrate a phototransistor which is capable of reaching a high gain-bandwidth product for high-speed applications. The proposed design criteria can be employed in conjunction with the engineering of the device size to achieve a wide tunability of the gain and bandwidth, hence paving the way toward fast photodetectors for applications with different light levels.

Phototransistors (PTs) are ideal for designing scalable, compact and highly sensitive optical detection systems, thanks to their large optical gains, low voltage operation, and compatibility with standard lithographic techniques and CMOS technology. Phototransistor diodes (PTDs), two-terminal, floating-base phototransistors, have been employed for designing photodetectors operating at wavelengths ranging from the infrared to the ultraviolet region of the electromagnetic spectrum.[1–3] Short-wavelength infrared (SWIR) PTDs based on an InGaAs absorption layer, as an example, have found applications in imaging,[4] optical coherence tomography (OCT) systems,[5] and chip-scale optical interconnections.[6]

Recently, interesting developments have come from PTDs based on nanoscale and low-dimensional (LD) materials, such as quantum dots (0-D),[7] nanowires (1-D),[8] and two-dimensional (2-D) detectors.[9,10] These devices have attracted ever-increasing attention thanks to their unmatched responsivity[11] and bandwidth,[12] potentially allowing them to reach single-photon sensitivity.[13] Indeed, shrinking the size of PTDs represents a primary strategy to increase both their gain and speed,[14] which in part explains the outstanding performance of these nanoscaled detectors.

In their most common implementations, PTDs are typically required to operate at optical power levels that can vary by several orders of magnitudes depending on their application. Since the gain of PTDs is a highly nonlinear function of the optical power,[15] it is therefore crucial to characterize and report the power dependency of the PTD performance, in order for these devices to find useful technological application. In this work, we seek to develop a clear physical understanding of the power dependency of the PTD gain-bandwidth

performance through a systematic investigation of the case of SWIR PTDs. We develop a simple physical model for explaining the experimental behavior which can guide the design of detectors tailored for the envisaged applications, and can readily be generalized for other types of PTDs.

The gain of PTDs is generated through transistor action: photogenerated excess carriers transport to the base layer and modulate its potential barrier, causing current multiplication of the majority carrier diffusing from the emitter (injector). This amplification mechanism is also common to most LD PTDs, as photogenerated carriers modulate a potential barrier such as at the contacts,[16] at the surface,[17] or at the interfaces.[18] As an example, the gain mechanisms in nanowire detectors were shown to be similar to that of either a floating-base junction PT or a floating gate field-effect PT.[8] The gain is therefore related to the excess carrier recombination lifetime at the base (or barrier) layer, τ_R, and to the base transit time of the majority carrier, τ_{t_B}[19]

$$\beta = \frac{\tau_R}{\tau_{t_B}}. \quad (1)$$

Notably, the carrier recombination lifetime is strongly dependent on the excess carrier concentration injected at the base.[20] Similarly, at higher current density the transit time is significantly increased by base charging and push-out such as in the Kirk effect.[21] As a result, the gain of PTDs is strongly dependent on the optical power, corresponding to the excess carrier injection level.[15]

The power dependency of PTD gain is characterized by two distinct regimes, as shown in Fig. 1. At low optical power levels, recombination of the photogenerated excess carriers constitutes the dominant contribution to limiting the gain. In particular, at very low light levels the gain of PTDs is constant with increasing optical power, since the number of photogenerated excess carriers is small compared to the intrinsic carrier concentration in the base. As their concentration further increases with the injection level, however, they begin saturating the recombination center sites at the base layer, resulting in an increase in gain. As a result, the gain is peaked at a given optical power and significantly drops away from it, hence establishing a limited range for high-gain operation of PTDs. The concentration of recombination centers (trap states) and the doping level of the base layer are therefore crucial parameters in determining the range of this high-gain operational regime.

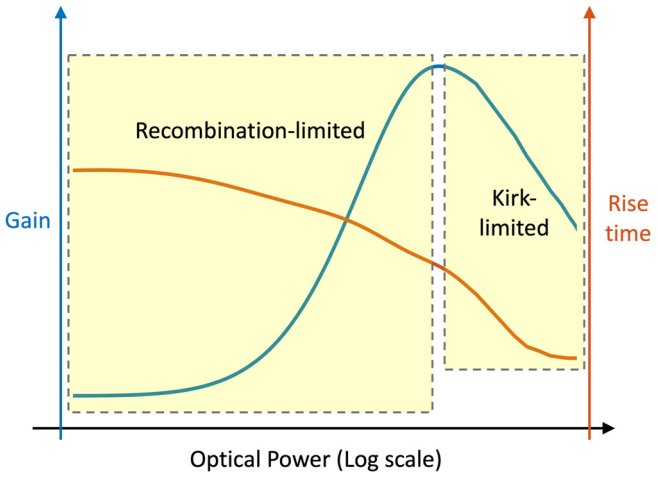

FIG. 1. Typical power dependency of gain (left axis) and rise time (right axis) of phototransistors, measured for an infrared PTD at 1550 nm. Two distinct regimes of operation are highlighted: one at lower optical power (denoted "recombination-limited regime"), and one at higher optical power levels, dominated by the Kirk effect[21] ("Kirk-limited regime").

In order to investigate the effects of these parameters and define useful design criteria to engineer the high-gain operational regime, we experimentally studied three heterojunction phototransistor (HPT) epitaxial structures encompassing different material systems and band properties. Figure 2 shows a schematic of the three structures, together with their simulated band diagrams at zero bias, in darkness.

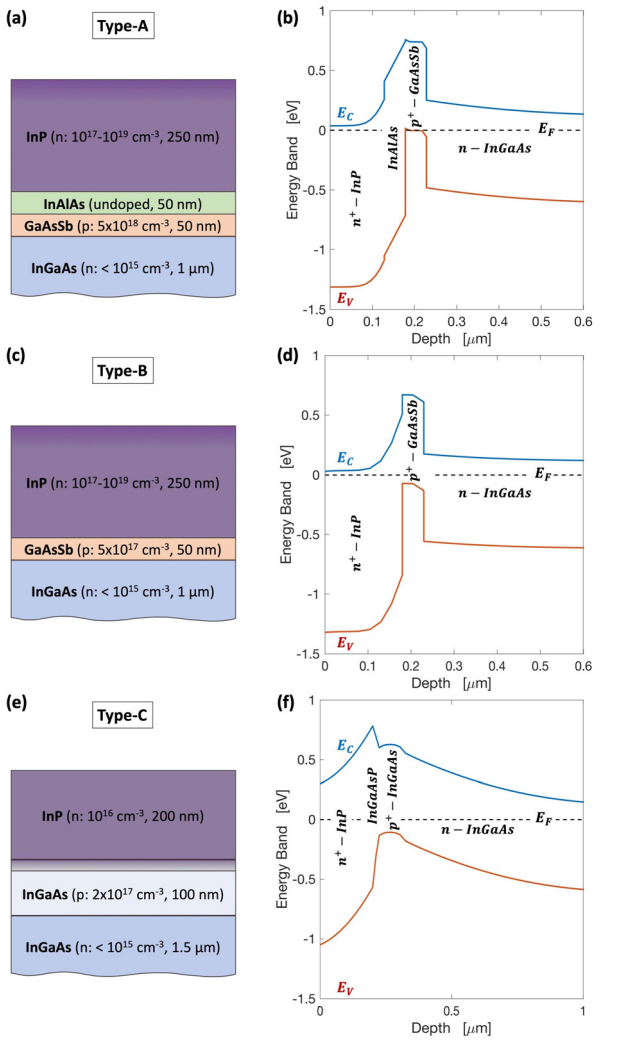

FIG. 2. Schematic of the epilayers of the three investigated PTD structures (a), (c), and (e) with the corresponding equilibrium energy band diagram in darkness, generated using ATLAS software (b), (d), and (f). In the schematic, "InGaAs" is used for denoting the $In_{0.53}Ga_{0.47}As$ material composition, "GaAsSb" for $GaAs_{0.52}Sb_{0.48}$, and "InAlAs" for $In_{0.52}Al_{0.48}As$. Panels (a) and (b) refer to the Type-A structure, (c) and (d) to the Type-B, and (e) and (f) to the Type-C. The shaded area in (e) represents an InGaAsP graded-composition transition layer.

The type-A structure design has been reported in several works[22] and is based on type-II band alignment comprising a p^+-$GaAs_{0.52}Sb_{0.48}$ hole-trapping layer and an $In_{0.52}Al_{0.48}As$ electron-blocking layer. This structure has been comprehensively studied with the aid of simulation tools to characterize the effects of several design parameters (such as the thickness, composition, and doping of the epitaxial layers) on the device performance.[23–25] The type-B structure is somewhat similar to that of type-A, where the $In_{0.52}Al_{0.48}As$ electron-blocking layer has been removed, and the doping of the trapping layer reduced to 5×10^{17} cm^{-3}. Finally, type-C structure consists of a heterojunction phototransistor (HPT), entirely based on the InP/InGaAs material system.[26,27] All three epitaxial structures are grown on an InP substrate using metal organic chemical vapor deposition (MOCVD).

The device fabrication process has been described in detail for each of the structures in previous works.[25,27] The wafers were patterned using standard lithographic and lift-off techniques to define the multilayer metal contacts. The devices were then formed using the metal stack as a hard mask, etching through the emitter and base layers and into the thick collector layer, with a combination of wet and dry etching. The fabricated devices are shown in Fig. 3. Different sizes of detectors were fabricated, as size scaling is known to increase the gain and speed of the device.[14] In this work, only the results from a single detector size (30 μm) are presented: a more detailed characterization of size-dependent effects will be the subject of a future work. The photoresponse measurements were performed using a calibrated pulsed laser source, with a peak emission wavelength of 1550 nm, to illuminate devices from the backside (through the transparent InP substrate). The time-resolved photoresponse was recorded for each device, varying the power of the laser and the pulse width. The laser power was calibrated using a power meter and the optical losses of the setup were measured using an antireflection- (AR)-coated calibrated PIN detector.

At the low-light level (Fig. 1), the gain of PTDs is dominated by the contribution from the recombination rate of the excess carriers, mostly taking place at recombination centers in the highly doped base layer and its interfaces (trap-assisted recombination).[28] These phenomena can be modeled using the Shockley-Read-Hall (SRH) model, assuming a parabolic energy distribution of the traps within the bandgap, $N_t = N_{t_A}(E_t - E_i)^2 + N_{t_C}$, where N_{t_A} and N_{t_C} are fitting parameters.[20] The SRH recombination rate for the i-th trap level in the bandgap associated with energy E_t can be expressed as

$$U_i = \frac{\sigma_n \sigma_p v_{th} N_t (n_0 \Delta p + p_o \Delta n + \Delta n \Delta p)}{\sigma_p \left(p_0 + \Delta p + n_i e^{\frac{E_i - E_t}{k_B T}}\right) + \sigma_n \left(n_0 + \Delta n + n_i e^{\frac{E_t - E_i}{k_B T}}\right)}, \quad (2)$$

where σ_n and σ_p are the capture cross sections of electrons and holes, v_{th} is their thermal velocity, N_t and E_t are the concentration and energy level of the i-th recombination center, and n_0, Δn, p_0, and Δp are the equilibrium and excess concentrations of electrons and holes, respectively. The excess carrier concentration (injection level) is related to the optical power by

$$\Delta n = \frac{R_i \Phi}{v_D A q}, \quad (3)$$

where $R_i = \beta \frac{\lambda q}{hc}$ is the responsivity in units of A/W, Φ is the optical power in W, v_D is the carrier diffusion velocity, A is the detector area, and q is the charge of the electron.

The total recombination rate is derived from the sum over all trap energy levels for all recombination centers within the bandgap, from which the recombination lifetime can be calculated as[20]

$$\tau_R = \frac{\Delta n}{\sum_i U_i}. \quad (4)$$

Using Eqs. (1) and (4), the PTD gain (or, equivalently, its responsivity) as a function of the optical power is then obtained.

The measured gain of the three PTD structures as a function of the optical power level is reported in Fig. 4. The presented SRH model

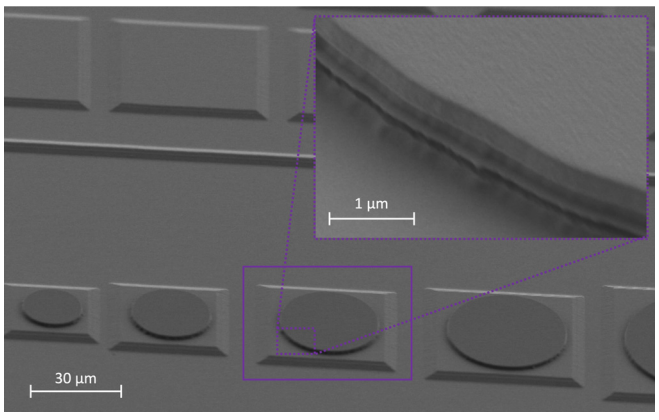

FIG. 3. Scanned electron microscopy image of a fabricated set of devices of different sizes: the measurements reported in this work correspond to a single device size (30 μm), such as that highlighted in the box. The devices in this picture correspond to the type-B structure: the details of the epitaxial layers, including the InGaAs collector, the GaAsSb base, the InP emitter, and the multilayer metal stack can be clearly seen in the inset.

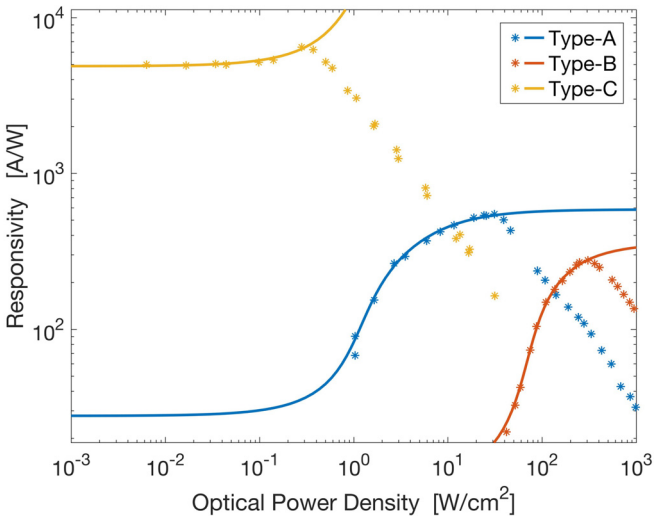

FIG. 4. Measured PTD responsivity as a function of the optical power level at 1550 nm for the three investigated structures and SRH recombination model fit (solid line) to the experimental data. The fitting parameters for the three structures are reported in Table I. The fitted model deviates from the experimental data after the onset of the Kirk effect at high optical power levels.

based on the known material electronic and transport parameters was fitted to the measured data using the unknown density and energy distribution of trap states as free fitting parameters. The model fitting is shown in Fig. 4 as solid lines, and the parameters resulting from the fitting are reported in Table I. As mentioned above, the SRH model deviates from the measured data points after the gain drop due to the onset of the Kirk effect. This effect is not included in the presented model, as will be the subject of future work.

The type-C HPT structure achieves the highest gain (∼2000), followed by type-A (∼200) and lastly type-B (∼90). The SRH model helps providing physical understanding of this behavior: the total trap concentration at the base layer, calculated from the fitting parameters as $N_T = \sum_i N_{t_i}$, is nearly three orders of magnitude lower for type-C structure than for type-A and type-B (and slightly higher for type-B than for type-A). These concentrations find plausible justification in the epitaxial and band design of the three structures, shown in Fig. 2. MOCVD of GaAsSb-based epitaxial structures is typically characterized by a higher defect density at the interfaces compared to HPTs based on the InGaAs/InP material system, typically related to Sb segregation and type-II band alignment.[29,30] Similarly, the higher trap concentration in type-B structures compared to type-A can be explained by the lack of the InAlAs transition layer, causing a more abrupt InP-GaAsSb type-II interface.

As shown in Fig. 4, the onset of the Kirk effect starts limiting the gain of the type-C structures at a much lower power (∼100 nW) than for type-A (∼10 μW) and type-B (∼100 μW). As a result, despite the large difference in gain between the three structures, each of them performs significantly better than the other two within a certain range of optical power. This is also reflected in the gain-bandwidth product (GBP) of the PTDs, shown in Fig. 5. Interestingly, the peak GBP is fairly similar (within an order of magnitude) for all three structures, despite the large difference in gain. This is because the bandwidth of PTDs typically increases with optical power, as shown in Fig. 1. Indeed, the carrier lifetime is known to affect both the gain and the response time of PTs;[31] hence, the increased density of trap states at the base that causes lower gain (such as for type-A and type-B structures) also allows for a faster device response. As a consequence, the structures with the highest gain are also the ones with the lowest bandwidth, a trade-off which highlights the importance of appropriate design of PTDs depending on the optical power level operation of the envisaged application. Finally, it is worth noting that although three-terminal phototransistor designs with higher GBP have been demonstrated,[32] such devices are not usually employed for high-sensitivity, low-noise photodetection, due to their high dark current and injection noise.

TABLE I. SRH model fitting parameters.

Structure	Type-A	Type-B	Type-C
Detector size	20 μm	20 μm	30 μm
Base doping (N_A)	5×10^{18} cm^{-3}	5×10^{17} cm^{-3}	2×10^{17} cm^{-3}
Total trap conc. (N_T)	6×10^{12} cm^{-3}	6.4×10^{12} cm^{-3}	7.5×10^{9} cm^{-3}
Max$\{\sigma_n, \sigma_p\}$	5×10^{-15} cm^2	5×10^{-15} cm^2	5×10^{-15} cm^2
τ_{tB}	10^{-10} s	10^{-10} s	2×10^{-10} s

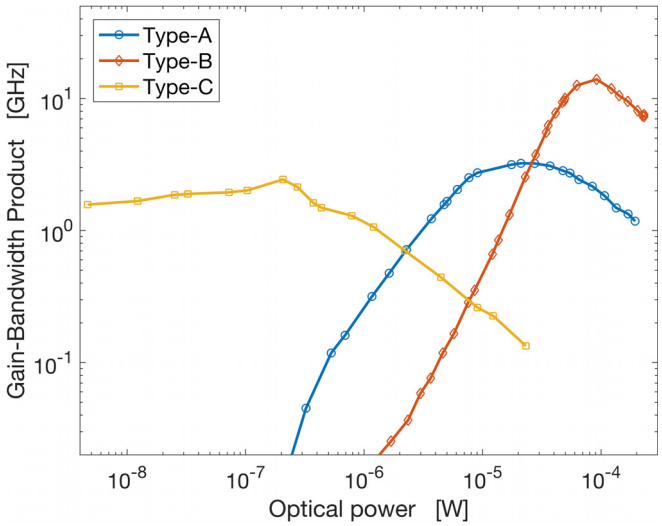

FIG. 5. Measured gain-bandwidth product of the three PTD structures investigated, as a function of the optical power illumination level at 1550 nm wavelength. *GBP* $= \beta/\tau_{rise}$. For a detailed comparison of the GBP of the presented devices with that of existing SWIR detectors from PT and other technologies, refer to Fig. S6 in the supplementary material.

In summary, we reported a case study of the gain and bandwidth as a function of optical power for three different short-wave infrared PTD architectures. The observed behavior can be explained using a Shockley-Read-Hall recombination model in combination with Kirk effect, based on the material properties. We maintain that PT band design and control of material quality allow to effectively engineer the high gain-bandwidth operation of PTDs at the desired optical power. The crucial design parameters are identified in the base doping and interface defect concentration. Most notably, the density of recombination centers at the base decreases the PTD gain at low light and increases the speed of the device. This physical understanding can be readily applied to PTDs operating at different wavelengths and based on different material systems, including low-dimensional and nanoscale detectors. We believe that the presented design criteria can be used to guide the development of useful PTD devices that satisfy the system requirements for the envisaged applications, capable of advancing the state of the art of the respective field.

See the supplementary material for details on the sensitivity and noise characterization, quantum efficiency, and the time-resolved photoresponse measurements of the reported devices, as well as a comparison of the reported GBP with that of competing SWIR technologies.

This work was partially supported by ARO Award No. W911NF1810429, and NIH Award No. 1R21EY029516-01. This work was performed, in part, at the Center for Nanoscale Materials of Argonne National Laboratory. Use of the Center for Nanoscale Materials, an Office of Science user facility, was supported by the U.S. Department of Energy, Office of Science, Office of Basic

Energy Sciences, under Contract No. DE-AC02-06CH11357. S.B. gratefully acknowledges support from the Ryan Fellowship and the International Institute for Nanotechnology at Northwestern University.

REFERENCES

[1]K.-J. Baeg, M. Binda, D. Natali, M. Caironi, and Y.-Y. Noh, "Organic light detectors: Photodiodes and phototransistors," Adv. Mater. **25**(31), 4267–4295 (2013).
[2]D. Jiang, L. Li, H. Chen, H. Gao, Q. Qiao, Z. Xu, and S. Jiao, "Realization of unbiased photoresponse in amorphous InGaZnO ultraviolet detector via a hole-trapping process," Appl. Phys. Lett. **106**(17), 171103 (2015).
[3]K.-W. Ang, M.-B. Yu, G.-Q. Lo, and D.-L. Kwong, "Low-voltage and high-responsivity germanium bipolar phototransistor for optical detections in the near-infrared regime," IEEE Electron Device Lett. **29**(10), 1124–1127 (2008).
[4]O. G. Memis, J. M. Kohoutek, W. Wu, R. M. Gelfand, and H. Mohseni, "A short-wave infrared nanoinjection imager with 2500 A/W responsivity and low excess noise," IEEE Photonics J. **2**, 858–864 (2010).
[5]V. Fathipour, T. Schmoll, A. Bonakdar, S. Wheaton, and H. Mohseni, "Demonstration of shot-noise-limited swept source OCT without balanced detection," Sci. Rep. **7**(1), 1183 (2017).
[6]K. T. Settaluri, S. Lin, S. Moazeni, E. Timurdogan, C. Sun, M. Moresco, Z. Su, Y.-H. Chen, G. Leake, D. LaTulipe, C. McDonough, J. Hebding, D. Coolbaugh, M. Watts, and V. Stojanović, "Demonstration of an optical chip-to-chip link in a 3D integrated electronic-photonic platform," in *ESSCIRC Conference 2015-41st European Solid-State Circuits Conference* (*ESSCIRC*) (IEEE, 2015), pp. 156–159.
[7]V. Adinolfi and E. H. Sargent, "Photovoltage field-effect transistors," Nature **542**(7641), 324 (2017).
[8]H. Zhang, A. Babichev, G. Jacopin, P. Lavenus, F. Julien, A. Yu. Egorov, J. Zhang, T. Pauporté, and M. Tchernycheva, "Characterization and modeling of a ZnO nanowire ultraviolet photodetector with graphene transparent contact," J. Appl. Phys. **114**(23), 234505 (2013).
[9]V. Ryzhii and M. Ryzhii, "Graphene bilayer field-effect phototransistor for terahertz and infrared detection," Phys. Rev. B **79**(24), 245311 (2009).
[10]N. Yavarishad, T. Hosseini, E. Kheirandish, C. P. Weber, and N. Kouklin, "Room-temperature self-powered energy photodetector based on optically induced Seebeck effect in Cd_3As_2," Appl. Phys. Express **10**(5), 052201 (2017).
[11]A. Zhang, H. Kim, J. Cheng, and Y.-H. Lo, "Ultrahigh responsivity visible and infrared detection using silicon nanowire phototransistors," Nano Lett. **10**(6), 2117–2120 (2010).
[12]W. S. Ko, I. Bhattacharya, T.-T. D. Tran, K. W. Ng, S. A. Gerke, and C. Chang-Hasnain, "Ultrahigh responsivity-bandwidth product in a compact InP nanopillar phototransistor directly grown on silicon," Sci. Rep. **6**, 33368 (2016).
[13]R. H. Hadfield, "Single-photon detectors for optical quantum information applications," Nat. Photonics **3**(12), 696 (2009).
[14]M. Rezaei, M. Park, C. L. Tan, and H. Mohseni, "Sensitivity limit of nanoscale phototransistors," IEEE Electron Device Lett. **38**(8), 1051–1054 (2017).
[15]A. Pfenning, F. Hartmann, F. Langer, M. Kamp, S. Höfling, and L. Worschech, "Sensitivity of resonant tunneling diode photodetectors," Nanotechnology **27**(35), 355202 (2016).
[16]Y. Hu, J. Zhou, P.-H. Yeh, Z. Li, T.-Y. Wei, and Z. L. Wang, "Supersensitive, fast-response nanowire sensors by using Schottky contacts," Adv. Mater. **22**(30), 3327–3332 (2010).
[17]C.-J. Kim, H.-S. Lee, Y.-J. Cho, K. Kang, and M.-H. Jo, "Diameter-dependent internal gain in ohmic Ge nanowire photodetectors," Nano Lett. **10**(6), 2043–2048 (2010).
[18]G. Wang, S. Chu, N. Zhan, Y. Lin, L. Chernyak, and J. Liu, "ZnO homojunction photodiodes based on Sb-doped p-type nanowire array and n-type film for ultraviolet detection," Appl. Phys. Lett. **98**(4), 041107 (2011).
[19]A. Rogalski, *Infrared Detectors* (CRC Press, 2010).
[20]D. L. Meier, J.-M. Hwang, and R. B. Campbell, "The effect of doping density and injection level on minority-carrier lifetime as applied to bifacial dendritic web silicon solar cells," IEEE Trans. Electron Devices **35**(1), 70–79 (1988).
[21]D. Zhou, D. Han, C. Sun, R. Yang, and K. Liang, "Low-threshold-switch phototransistor based on kirk effect and float-zone silicon," Appl. Phys. Lett. **90**(11), 113513 (2007).
[22]V. Fathipour, I. H. Nia, A. Bonakdar, and H. Mohseni, "On the sensitivity of electron-injection detectors at low light level," IEEE Photonics J. **8**(3), 1–7 (2016).
[23]Y. Movassaghi, V. Fathipour, M. Fathipour, and H. Mohseni, "Analytical and numerical evaluation of electron-injection detector optimized for SWIR photon detection," J. Appl. Phys. **121**(8), 084501 (2017).
[24]Y. Movassaghi, V. Fathipour, M. Fathipour, and H. Mohseni, "Analytical modeling and numerical simulation of the short-wave infrared electron-injection detectors," Appl. Phys. Lett. **108**(12), 121102 (2016).
[25]V. Fathipour, S. J. Jang, I. H. Nia, and H. Mohseni, "Impact of three-dimensional geometry on the performance of isolated electron-injection infrared detectors," Appl. Phys. Lett. **106**(2), 021116 (2015).
[26]M. Rezaei, M.-S. Park, C. L. Tan, C. Rabinowitz, S. Wheaton, and H. Mohseni, "Heterojunction phototransistor for highly sensitive infrared detection," in *Infrared Technology and Applications XLIII* (International Society for Optics and Photonics, 2017), Vol. 10177, p. 101771O.
[27]M.-S. Park, M. Razaei, K. Barnhart, C. L. Tan, and H. Mohseni, "Surface passivation and aging of InGaAs/InP heterojunction phototransistors," J. Appl. Phys. **121**(23), 233105 (2017).
[28]F. Callewaert, A. Hoang, and M. Razeghi, "Generation-recombination and trap-assisted tunneling in long wavelength infrared minority electron unipolar photodetectors based on InAs/GaSb superlattice," Appl. Phys. Lett. **104**(5), 053508 (2014).
[29]Y. Wei and M. Razeghi, "Modeling of type-II InAs/GaSb superlattices using an empirical tight-binding method and interface engineering," Phys. Rev. B **69**(8), 085316 (2004).
[30]T. Wosiński, A. Makosa, T. Figielski, and J. Raczyńska, "Deep levels caused by misfit dislocations in GaAsSb/GaAs heterostructures," Appl. Phys. Lett. **67**(8), 1131–1133 (1995).
[31]J. P. Helme and P. A. Houston, "Analytical modeling of speed response of heterojunction bipolar phototransistors," J. Lightwave Technol. **25**(5), 1247–1255 (2007).
[32]S. Chandrasekhar, M. K. Hoppe, A. G. Dentai, C. H. Joyner, and G. J. Qua, "Demonstration of enhanced performance of an InP/InGaAs heterojunction phototransistor with a base terminal," IEEE Electron Device Lett. **12**(10), 550–552 (1991).